

Figure S1. XRD patterns for ISPC 80/ Cloisite 30B (5.0 wt%) nanocomposite.

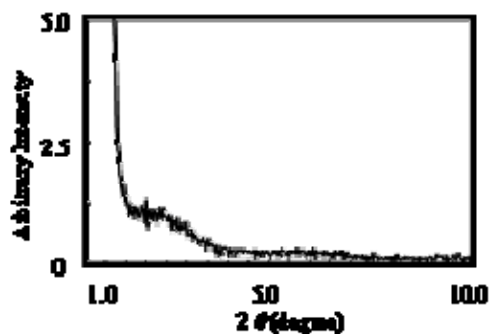


Figure S2. XRD patterns for ISPC 90/ Cloisite 30B (5.0 wt%) nanocomposite.

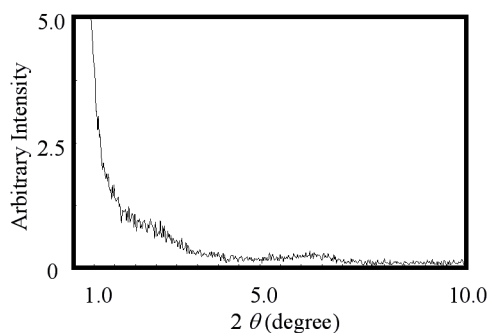


Figure S3. XRD patterns for ISPC 98/ Cloisite 30B (5.0 wt%) nanocomposite.

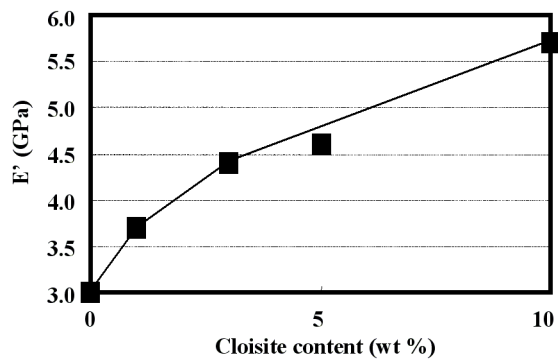


Figure S4. The variation of the storage modulus (E') of the ISPC 80/Cloisite 30B nanocomposite at various concentrations of Cloisite 30B.

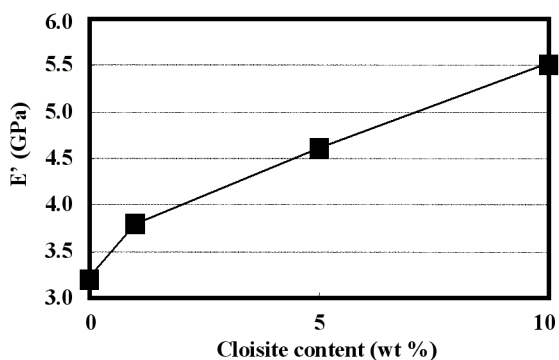


Figure S5. The variation of the storage modulus (E') of the ISPC 90/Cloisite 30B nanocomposite at various concentrations of Cloisite 30B.

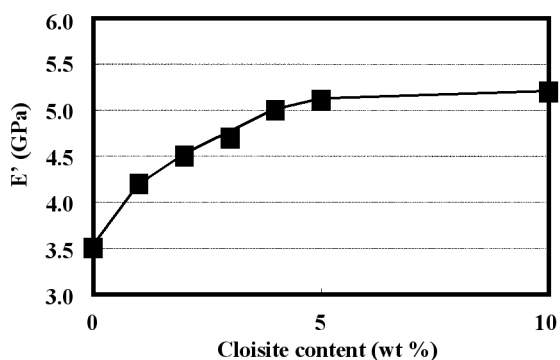


Figure S6. The variation of the storage modulus (E') of the ISPC 98/Cloisite 30B nanocomposite at various concentrations of Cloisite 30B.

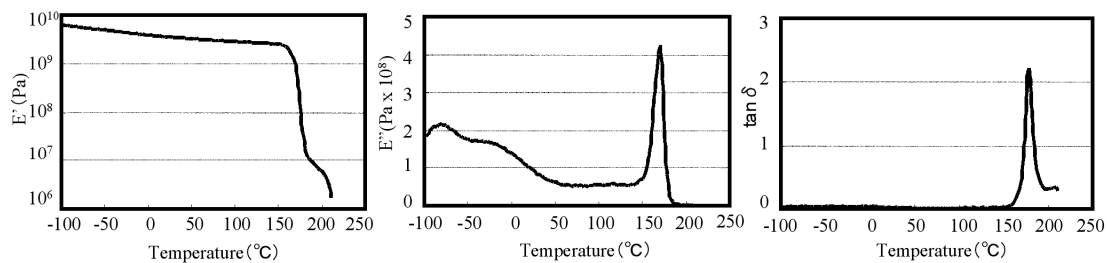


Figure S7. Temperature dependence of E' , E'' , and $\tan \delta$ for the neat ISPC 95.

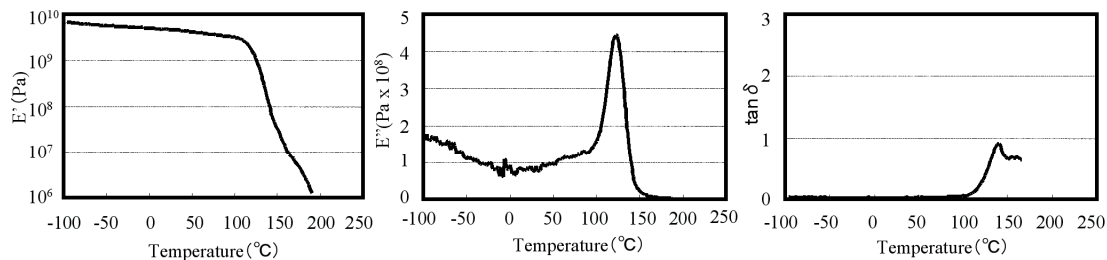


Figure S8. Temperature dependence of E' , E'' , and $\tan \delta$ for the ISPC 80/Cloisite 30B (5.0 wt%) nanocomposite.

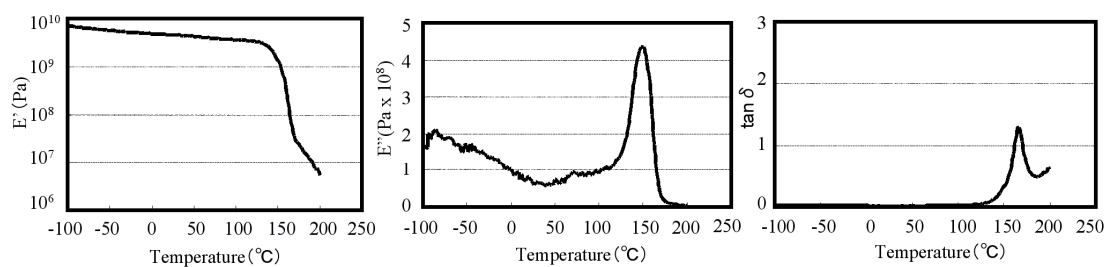


Figure S9. Temperature dependence of E' , E'' , and $\tan \delta$ for the ISPC 90/Cloisite 30B (5.0 wt%) nanocomposite.

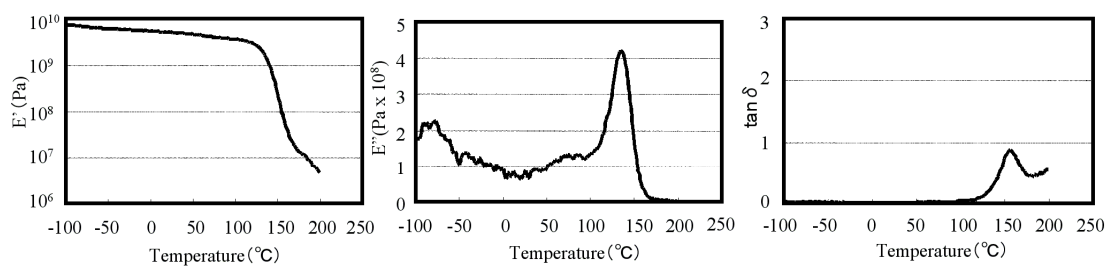


Figure S10. Temperature dependence of E' , E'' , and $\tan \delta$ for the ISPC 98/Cloisite 30B (5.0 wt%) nanocomposite.